

NJC

Accepted Manuscript



This article can be cited before page numbers have been issued, to do this please use: L. F. Loguercio, C. F. de Matos, M. C. de Oliveira, G. Marin, S. Khan, N. M. Balzaretto, J. Dupont, M. J. L. José Leite Santos and J. Ferreira, *New J. Chem.*, 2018, DOI: 10.1039/C8NJ02431F.



This is an Accepted Manuscript, which has been through the Royal Society of Chemistry peer review process and has been accepted for publication.

Accepted Manuscripts are published online shortly after acceptance, before technical editing, formatting and proof reading. Using this free service, authors can make their results available to the community, in citable form, before we publish the edited article. We will replace this Accepted Manuscript with the edited and formatted Advance Article as soon as it is available.

You can find more information about Accepted Manuscripts in the [author guidelines](#).

Please note that technical editing may introduce minor changes to the text and/or graphics, which may alter content. The journal's standard [Terms & Conditions](#) and the ethical guidelines, outlined in our [author and reviewer resource centre](#), still apply. In no event shall the Royal Society of Chemistry be held responsible for any errors or omissions in this Accepted Manuscript or any consequences arising from the use of any information it contains.

Synergistic interplay of ionic liquid and dodecyl sulphate driving the oxidation state of Polypyrrole based electrodes

Lara F. Loguercio,^a Carolina F. de Matos,^b Matheus C. de Oliveira,^a Graciani Marin,^a Sherdil Khan,^c Naira M. Balzaretto, Jairton Dupont,^a Marcos J. Leite Santos,^{a*} Jacqueline F. Leite Santos^{a*}

Received 00th January 20xx,
Accepted 00th January 20xx

DOI: 10.1039/x0xx00000x

www.rsc.org/

Herein, polypyrrole (PPy) films are prepared via electrochemical deposition in a mixture of 1-n-butyl-3-methylimidazolium methanesulfonate (BMI.CH₃SO₃) ionic liquid (IL) and dodecyl sulfate (DS). The physico-chemical properties of the films have been investigated by a wide range of characterization techniques. PPy films synthesized in DS or IL have shown larger and irregular granules as compared to PPy films prepared in the mixture of DS and IL. This result is related to the preferential dissolution of pyrrole monomers in micelle templates formed by the IL and a co-assembly of IL and dodecyl-sulfate (DS); thereby, decreasing granule size and affecting the structural arrangement of the polymer chain. The template behavior of IL in combination with DS promotes the selective formation of polaron and bipolaron states in the PPy films. This effect has been investigated by UV-Vis spectrophotometry, Raman spectroscopy, electrochemical impedance spectroscopy (EIS), cyclic voltammetry, scanning electron microscopy, transmission electron microscopy, and electrical conductivity measurements. The synergy of IL-DS has helped to decrease the resistivity of PPy film from 2.17×10² Ω cm for PPy-IL to 2.44 Ω for PPy-IL-DS. EIS has also shown, a decreased interfacial charge transfer resistance for PPy-IL-DS, when compared to PPy-IL. The cyclic voltammetry curves have shown that PPy films are electrocatalytically active for I⁻/I₃⁻ redox reaction and therefore, applied as a counter electrode (CE) in dye sensitised solar cells. The PPy based CEs resulted in nearly the same photocurrent and energy conversion efficiencies as that obtained from conventional Pt CE.

1. Introduction

Polypyrrole is an intrinsically conducting polymer; widely studied in hybrid materials with other semiconductors,^{1,2} metallic nanoparticles³ and for applications in chemical sensors,⁴⁻⁶ biosensors,⁴ electrochemical capacitors and supercapacitors,⁷ electrochromic devices⁸⁻¹⁰, batteries^{11,12} and, more recently to replace platinum nanoparticles in dye sensitised solar cells.^{13,14} Conducting polymers are particularly interesting to use as a counter electrode in DSSCs due to the combination of low cost, high conductivity, good stability, high specific capacitance, optical transparency in the visible-light region, in addition to a catalytic activity for triiodide reduction

and charge-transfer ability.¹⁵

Physico-chemical properties of a conducting polymer can be understood by its oxidation level.^{16,17} It is well established that optical and electronic properties of PPy are dependent on the presence of polaron and bipolaron states. Hence, doping and undoping effects influence these states; thereby, affecting the conductivity, optical, and electronic properties of the film. The literature reports on controlling polaron and bipolaron states and monitoring the conducting polymer oxidation states.¹⁸⁻²⁰ Polaron and bipolaron states are associated with intermediate energy levels that arise within the electronic band gap region of a polymer due to oxidation followed by doping. The polymeric chain has to accommodate charges created by oxidation and accommodation of these extra charges involves conformational and structural changes.^{21,22} Use of different doping agents has been found to result in different optical and structural properties.^{21,23-28}

Ionic liquid (IL) assisted electrochemical synthesis of PPy has gained a considerable attention.²⁹⁻³¹ Addition of ILs such as (1-butyl-3-methylimidazolium bis(trifluoromethylsulfonyl)imide and 1-ethyl-3-methylimidazolium bis(perfluoroethanesulfonyl)imide has improved morphological and mechanical properties of PPy. Most of the literature reports the synthesis of PPy films adding only one IL and comparing the films to PPy obtained in conventional electrolytes. On the other hand, there is plenty of literature showing the effects of Dodecyl sulphate (DS) on PPy films.³²⁻³⁴

[a] MS L. F. Loguercio, Mr. M. C. de Oliveira, Dr. G. Marin, Prof. Dr. M. J. L. Santos, Prof. Dr. J. F. L. Santos, Prof. Dr. Jairton Dupont
Instituto de Química, Universidade Federal do Rio Grande do Sul, CEP 91501-970, Porto Alegre, RS, Brazil

[b] Prof. Dr. C. de Matos
Campus Caçapava do Sul, Universidade Federal do Pampa, CEP 96570-000, Caçapava do Sul, RS, Brazil

[c] Prof. Dr. S. Khan, Prof. Dr. N. M. Balzaretto
Instituto de Física, Universidade Federal do Rio Grande do Sul, CEP 91501-970, Porto Alegre, RS, Brazil

† Footnotes relating to the title and/or authors should appear here.
Electronic Supplementary Information (ESI) available: [details of any supplementary information available should be included here]. See DOI: 10.1039/x0xx00000x

Therefore, it is important to investigate the electrochemical polymerization of PPy in a mixture of ionic liquid and DS aiming to improve structural and catalytic properties of PPy.

In this work, a synergistic effect resulting from the electrochemical synthesis of PPy films in solution containing a mixture of 1-butyl-3-methylimidazolium methanesulfonate (BMI.CH₃SO₃) IL and sodium dodecyl sulfate (DS) is demonstrated. The films were applied as an alternative counter electrode to assemble DSSC, which are Pt-free, retaining high electron transportation and catalytic activity.

2. Experimental

Pyrrole monomer (Py) was double distilled and stored in N₂ at 4 °C. Sodium dodecyl sulfate (SDS), gold (II) chloride solution (HAuCl₄), 1-methylimidazole (C₄H₆N₂), butyl methanesulfonate (C₅H₁₂O₃S), acetone, sodium iodate (NaI), iodine (I₂), acetonitrile (CH₃CN), 1-butyl-3-methylimidazolium iodide (BMII, C₈H₁₅IN₂), guanidinium thiocyanate, 4-ter-butylpyridine (C₉H₁₃N), and valeronitrile (CH₃(CH₂)₃CN) were obtained from Aldrich. Anhydrous lithium perchlorate (LiClO₄) was purchased from Dinâmica. All reagents were used as received. Fluorine-doped tin oxide (FTO glass, 15 Ω cm⁻²) was obtained from Solaronix. All aqueous solutions were prepared with ultrapure water (Milli-Q).

2.1 Syntheses of 1-Butyl-3-methylimidazolium methanesulfonate (BMI.CH₃SO₃)

A mixture of 1-methylimidazole (77.18 g, 0.940 mol) and butyl methanesulfonate (143.07 g, 0.940 mol) was kept at room temperature using an external water bath for 72 h. The resulting crystalline mass of crude 1-butyl-3-methylimidazolium methanesulfonate was recrystallized twice using acetone as a solvent (1 mL solvent / g 1-butyl-3-methylimidazolium methanesulfonate). Drying under reduced pressure yielded very hygroscopic colourless crystals (222.30 g, 95 %) with mp 77.1 °C. ¹H NMR (400 MHz, D₂O): δ ppm = 8.76 (s, 1H), 7.53 (t, J = 4.0 Hz, 1H), 7.48 (t, J = 4.0 Hz, 1H), 4.24 (t, J = 8.0 Hz, 1H), 3.94 (s, 3H), 2.82 (s, 3H), 1.89 (qui, 2H), 1.35 (sex, J = 8.0 Hz, 2H), 0.96 (t, J = 8.0 Hz, 3H). ¹³C NMR (101 MHz, D₂O): δ ppm = 135.79, 123.46, 122.19, 49.33, 38.53, 35.61, 31.23, 18.72, 12.64. The ionic liquid 1-butyl-3-methylimidazolium methanesulfonate (BMI.CH₃SO₃) used in the syntheses of PPy films is labelled IL.

2.2 Synthesis of PPy thin films

PPy-based films were electrochemically polymerised in a three electrode cell at room temperature using an Autolab 302N potentiostat. Fluorine doped tin oxide (FTO) glass substrates were used as working electrodes, a platinum wire was used as a counter electrode, and Ag/AgCl was used as the reference electrode. The films were synthesised by performing one voltammetric cycle from -0.3 to +1.3 V at a scan rate of 30 mV s⁻¹. The synthesis solutions were i) 0.1 mol L⁻¹ pyrrole and 0.1 mol L⁻¹ IL (PPy-IL) ii) 0.1 mol L⁻¹ pyrrole and 0.1 mol L⁻¹ DS (PPy-DS) iii) 0.1 mol L⁻¹ pyrrole, 0.1 mol L⁻¹ IL, and 0.1 mol L⁻¹

DS (PPy IL-DS), and iv) 0.1 mol L⁻¹ pyrrole, 0.1 mol L⁻¹ IL, 0.1 mol L⁻¹ DS, and 0.6 mmol L⁻¹ HAuCl₄ (PPy-IL-DS-AuNPs).

2.3 DSSC Assembling

TiO₂ pastes were screen-printed on a transparent conductive substrate (fluorine-doped tin oxide – FTO) previously soaked in 40 mmol L⁻¹ TiCl₄ aqueous solution at 80 °C for 30 min. The substrate was heated on a hot plate at 125 °C for 20 min and at 450 °C for 30 min in a tubular oven. The mesoporous TiO₂ electrode was immersed in 0.5 mmol L⁻¹ cis bis(isothiocyanato) bis(2,20 -bipyridyl-4,40 -dicarboxylato)-ruthenium(II) N-719 solution of acetonitrile/tertbutyl alcohol (1 : 1 v/v) and kept at room temperature for 24 h. Two kinds of counter electrodes were obtained: i) standard platinum-based counter electrodes were prepared by coating the FTO surface with 30 μL of 1 mmol L⁻¹ hexachloroplatinic acid and heating at 400 °C, and ii) PPy-based counter electrodes were obtained as described previously. The mediator responsible for regeneration of the dye was placed between the dye sensitised photoanode and the counter electrode. The device was sealed using a low melting temperature polymeric film (Meltonix). The electrolyte was 0.6 mol L⁻¹ BMII, 0.03 mol L⁻¹ I₂, 0.10 mol L⁻¹ guanidinium thiocyanate, and 0.5 mol L⁻¹ 4-ter-butylpyridine in a mixture of acetonitrile and valeronitrile.

2.4 Characterisation

Morphology was studied by scanning electron microscopy (SEM) using an EVO50 - Carl Zeiss microscope at 15 kV and transmission electron microscopy (TEM) using a JEOL JEM 1200 ExII. The mass content of Au NPs in the film was estimated from TEM images. Firstly, the average number of NPs was counted from a series of TEM images for PPy-IL-DS-AuNPs film for an area of 1 cm². Considering the spherical shape, the volume of the NPs was estimated from the average diameter of Au NPs. This volume was divided by the Au unit cell volume and multiplied by the number of atoms in the unit cell (four) to obtain the total number of atoms in each NP. Finally, using the Avogadro number, the mass content was estimated from the total number of atoms present in 1 cm² of the film area. Profile studies were performed using a Veeco Dektak 150. UV-VIS-NIR spectrophotometry was carried out with a Carry 5000. Infrared spectroscopy was carried out in attenuated total reflectance mode (FTIR-ATR) using a Bruker model Alpha-P. Raman spectra were obtained with an Olympus microscope, a single-pass monochromator, and a charge-coupled device (CCD) detector cooled with liquid nitrogen. Excitation was provided by 632.8 nm radiation from a 10 mW polarised He-Ne laser focused to a ~2 μm diameter spot. The laser beam was directed to the sample through the microscope objective by a holographic beam splitter. The scattered light was collected in back-reflection geometry through the same objective and filtered with a super-notch filter (HSNF-633-1.0, Kaiser Optical Systems). Grazing angle XRD was recorded by Shimadzu, Maxima XRD7000 diffractometer with an incident angle of 0.5° with Cu Kα radiation (λ = 1.54 Å) at 2θ° angle ranging from 10° to 80° with a step size of 0.05° and measuring time of 5 s per step using Bragg–Brentano geometry. The electrical resistivity

of the PPy films was measured by the four-point technique using a JANDEL Universal probe. The distance between points was fixed at 1.0 mm. Cyclic voltammetry curves were obtained over a potential range from -1.0 to +1.0 V vs Ag/AgCl at a scan rate of 30 mV s⁻¹. The electrolyte was 0.1 mol L⁻¹ LiClO₄ solution. The electrocatalytic activity for the I⁻/I³⁻ redox couple was evaluated by cyclic voltammetry over a potential range from -0.6 to 1.3 V at a scan rate of 20 mV s⁻¹ using 0.1 mol L⁻¹ LiClO₄, 10.0 mmol L⁻¹ NaI, and 1.0 mmol L⁻¹ I₂ in acetonitrile solution. Electrochemical impedance spectroscopy (EIS) was performed under AM 1.5 G filtered 100 mW cm⁻² illumination from a 300 W Xenon arc lamp at -0.8 V over a frequency range of 100 kHz to 100 mHz at a signal amplitude of 10 mV using Autolab, PGSTAT100. The performance of the DSSCs was evaluated by current versus potential measurements and incident photon to current efficiency (IPCE). Measurements were carried out using a 300 W Xenon arc lamp, using AM1.5 filter, with light intensity calibrated to 100 mW cm⁻² and recorded by a picoammperemeter Keithley, model 2400.

3. Results and discussion

3.1 Morphological characterisation

Figures 1 and S1 show SEM images of PPy films doped with different anions (PPy-DS, PPy-IL, and PPy-IL-DS) and embedded with gold nanoparticles (PPy IL-DS-AuNP).

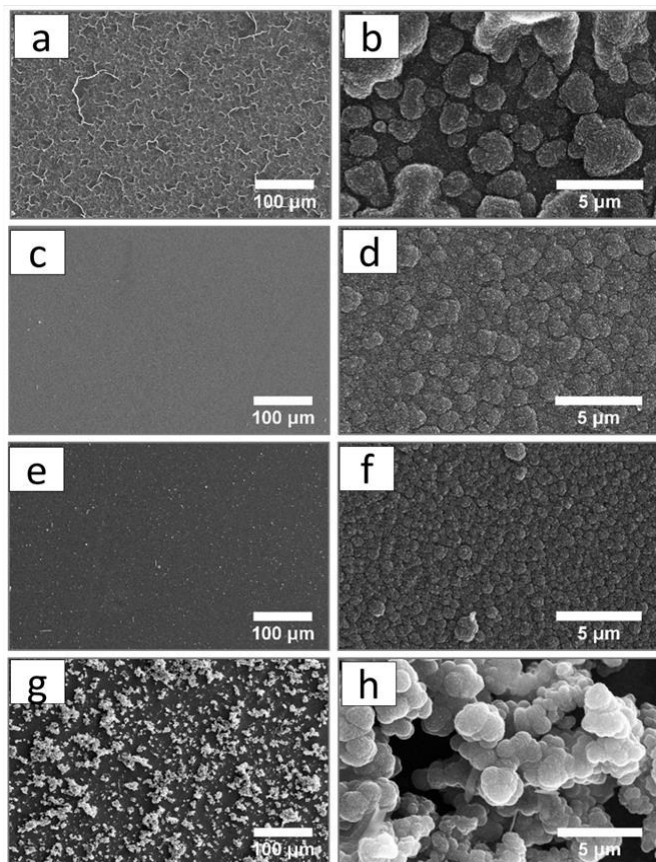


Figure 1. SEM images of (a-b) PPy-IL, (c-d) PPy-DS, (e-f) PPy-IL-DS and (g-h) PPy-IL-DS-AuNP films.

The film synthesised in IL (PPy IL) consists of large granules, up to 5 μm in size, resulting in a rough film with an average thickness of 341 ± 28 nm. This morphology can be related to the surfactant behaviour of the ionic liquid, which produces well-defined aggregated structures in aqueous media³²⁻³⁴ that act as micro- or nano-reactors, promoting the electropolymerisation of PPy on the electrode surface. The addition of DS as a counter-ion in the electrolyte yields closely packed PPy granules of decreased size (Figures 1c-f), resulting in more homogeneous and smooth films with average thicknesses of 48 ± 2 nm and 250 ± 118 nm for PPy-DS and for PPy-IL-DS, respectively. Interestingly, the PPy granules in PPy-DS-IL are smaller than in PPy-DS and PPy-IL, which is probably related to the change in the critical micelle concentration of DS in the presence of IL or due to the co-assembling of surfactant/ionic liquid mixtures as a result of a mixed micelle formation.³⁴⁻³⁶ Due to its hydrophobic nature, the PPy monomer is preferentially dissolved in these micelle assemblies.³⁶ Hence, in addition to doping, the presence of IL affects the size and structural arrangement of PPy during electrochemical synthesis. Indeed, the pronounced self-organisation of IL is widely used in the synthesis of self-assembled, highly organised hybrid nanostructures with unparalleled quality.³⁷ In Figure 1g and 1h, a significant change in morphology can be observed resulting from the presence of Au nanoparticles and the formation of larger PPy granules forming rougher films (average thickness 352 ± 47 nm). Once metallic nanoparticles present a large concentration of electrons at the surface, the embedded nanoparticles can act as adsorption centres for the oxidised pyrrole monomers and oligomers, driving the polymer chains to grow on the surroundings.³⁸ This is an interesting morphological feature for application in DSSC, as higher roughness indicates an improvement in surface area which should enhance the triiodide regeneration process. The presence of gold nanoparticles with an average crystallite size of 21.8 nm was confirmed by X-ray diffractometry (Figure S2a) and TEM (Figures S2b and S2c). The TEM images show AuNPs homogeneously distributed on the PPy film. Figure S2c shows the embedded and surrounded AuNPs in the PPy matrix, supporting the idea that the polymer grows around the AuNPs. The estimated mass content of AuNPs was found as ca. 0.5 μg of gold/cm².

3.2 Optical Characterisation

Figure 2 compares the UV-Vis-NIR spectra of the films. The absorption modes and the relative intensities are affected by the presence of IL and/or DS species. Two absorption bands, one at low energy (ca. 1.1 eV) and another at high energy (2.6-2.8 eV), are attributed to bipolaron states. The band at ca. 1.1 eV is assigned to the electron transition from the valence band to the bonding bipolaron state, while the band at ca. 2.7 eV is assigned to the transition from the valence band to the antibonding bipolaron state of PPy.^{32,39} The band at ca. 1.4 eV is related to the transition between bonding and antibonding

polaron states, which eventually recombine into more thermodynamically stable bipolarons.^{23,28,32}

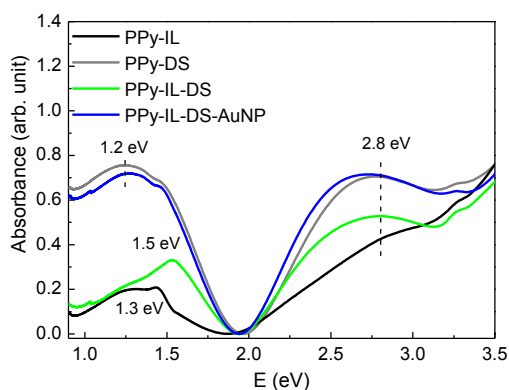


Figure 2. UV-Vis-NIR spectra of PPy-IL, PPy-DS, PPy-IL-DS, and PPy-IL-DS-AuNP films.

By comparing the relative intensities of the two main absorption modes, one can observe that PPy films have different oxidation levels depending on the presence of IL and/or DS. According to the literature an increase in band intensity near 1.0 eV is accompanied by an increase in electrical conductivity of the neutral polymer, reflecting partial oxidation.³² From these results it is possible to observe that DS doping promotes formation of bipolaron bands, while IL promotes polarons, and the mixture of DS and IL, as dopants, promotes an intermediate doping level of both polarons and bipolarons. Comparing the UV-Vis spectra of PPy-DS and PPy-DS-IL-AuNP no significant changes can be observed, suggesting that DS molecules are the main doping species. On the other hand, IL can act as template for the dispersion and stabilisation of metallic nanoparticles.⁴⁰ This behaviour is probably related to the weaker Lewis base character of methanesulfonate compared to sulfate. These results strongly suggest that doping with DS is affected by IL and is minimised by the presence of gold nanoparticles.

3.3 Structural characterisation

FTIR-ATR spectra of the films were acquired within the range of 1800-750 cm^{-1} (Figure S3). The characteristic vibrational modes of PPy are observed at 1527 cm^{-1} related to N-H stretching, at 1052 cm^{-1} , 1273 cm^{-1} , 1010 cm^{-1} , and 960 cm^{-1} , related to angular deformations in the plane of C-H, N-H, and C-N-C bonds in the oxidised pyrrole ring.^{41,42} According to the literature, the presence of certain vibrational modes can be used to indicate the oxidation state of PPy (polaron or bipolaron). The presence of IL molecules is confirmed by the band at 1636 cm^{-1} , which is assigned to the vibrational mode of 1-methyl imidazolium cations, and the band at 1573 cm^{-1} , which is assigned to stretching of the C=C and C=N bonds of

the imidazole ring.^{9,43} In addition, the vibrational mode at 1180 cm^{-1} observed in PPy-IL is attributed to ring deformation associated with the bipolaron state due to the presence of the IL.⁴³ In the spectrum of PPy-IL some bands are shifted compared to the spectrum of pure IL, suggesting an interaction between the PPy chains and the IL molecules. Due to the small amount of DS compared to PPy, the DS vibrational modes are hidden in the PPy spectrum. The bands at 1219 and 1080 cm^{-1} in the films containing DS are related to asymmetric and symmetric stretching modes of SO_4^{4-} , respectively.⁴⁴ Interestingly, the vibrational modes of the IL are not evident in the spectra of PPy-IL-DS and PPy-IL-DS-AuNP, suggesting that DS molecules are the main species in PPy doping. This data corroborates the oxidation levels observed in Figure 2.

Raman spectra of the films (Figure 3) were acquired over a range of 500-2000 cm^{-1} . All of the films exhibit vibrational bands characteristic of oxidised PPy.¹⁷ Two of the most important bands are observed at ca. 934 and 984 cm^{-1} . The band at ca. 984 cm^{-1} is related to the quinoid form of the pyrrole ring (reduced form) while the band at 934 cm^{-1} is associated with the benzoid ring (oxidised state).^{17,23,45}

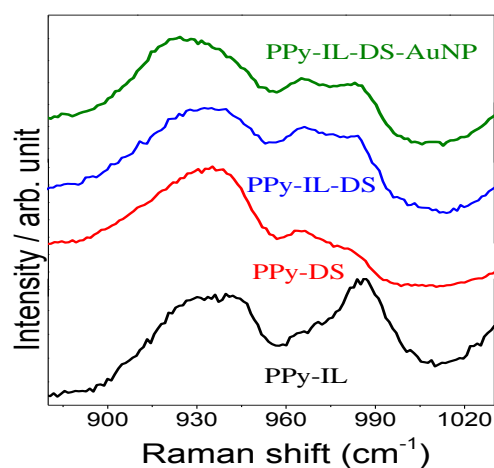


Figure 3. Raman spectra of PPy-IL, PPy-DS, PPy-IL-DS and PPy-IL-DS-AuNP-films.

In the spectrum of PPy-DS, the band at 934 cm^{-1} is much more intense than at ca. 990 cm^{-1} , demonstrating that oxidised state is predominant in this film. The presence of vibrational modes characteristic of the reduced state, in the oxidised polymer, is related to a range of conjugation lengths in the polypyrrole. Hence this spectrum strongly suggests the formation of bipolaron state in the PPy-DS film.^{24,46} However, for PPy-IL the vibrational mode at 984 cm^{-1} is slightly more intense than at 934 cm^{-1} , which have been related to a spectroscopy signature for the polaron state in PPy films.¹⁷ By mixing DS and IL one can observe an interplay of the dopants, resulting in an intermediary doping level, slightly more oxidised than for PPy-IL. The presence of gold nanoparticles increases the ratio

between the intensities of 934 cm^{-1} and 984 cm^{-1} , corroborating the discussion related to the optical characterisation (Figure 2).

3.4 Electrical characterization

The electrical resistivity of the films was compared with the oxidation (doping) level of the films (Figure S4). The values obtained in this work are consistent with previous works on electrochemically synthesised PPy films.^{31,47,48} The polaronic characteristic of PPy-IL, presenting pyrrole rings in the benzoid form (reduced form) observed by Raman spectroscopy, resulted in a more resistive film ($2.17 \times 10^2\ \Omega\ \text{cm}$) when compared to the other films. The highest conductivity was obtained for PPy-DS ($0.81\ \Omega\ \text{cm}$), which is in agreement with the high degree of oxidation observed by Raman spectroscopy. PPy-IL-DS and PPy IL-DS-AuNP are slightly more resistive than PPy-DS, with $2.44\ \Omega\ \text{cm}$ and $2.34\ \Omega\ \text{cm}$, respectively, however still more conductive than PPy-IL, again indicating that DS is the preferred dopant in films containing both agents. In addition, these results corroborate with the increase in band intensity at ca. $1.0\ \text{eV}$ observed in Figure 2.

3.5 Electrochemical characterisation

Cyclic voltammetric (CV) curves of the films (in $0.1\ \text{mol L}^{-1}\ \text{LiClO}_4$ at a scan rate of $30\ \text{mV s}^{-1}$) are found remarkably dependent on the doping agent used during the syntheses (Figure S5a). Table 1 shows the influence of doping agents on the intensities of cathodic (I_{pc}) and anodic (I_{pa}) peak currents and peak-to-peak separation (ΔE_p). ΔE_p values for all samples indicate a quasi-reversible system. The presence of AuNPs resulted in over 100% increase in charge density compared to PPy-IL and PPy-DS, and 30% increase compared to PPy-IL-DS. The interaction between PPy and Au NPs may affect the mobility of the dopant inside the polymer film, leading to an increase in the external voltage required for the redox process.

Table 1. Electrochemical parameters obtained from voltammograms of films (Figure S5).

Parameters	PPy-IL	PPy-DS	PPy-IL-DS	PPy-IL-DS-AuNP
E_g (V)	0.55	0.48	0.36	0.33
I_{pa} (mA cm^{-2})	0.33	0.32	0.61	0.80
E_{pa} (V)	0.52	0.76	0.90	0.76
I_{pc} (mA cm^{-2})	-0.36	-0.25	-0.45	-0.63
E_{pc} (V)	-0.07	-0.08	-0.16	-0.15
ΔE_p (V)	0.60	0.84	1.06	0.91
$(E_a + E_c)/2$ (V)	0.23	0.34	0.37	0.30
$ I_{pa} / I_{pc} $	0.92	1.28	1.35	1.27

Removal of electrons from the occupied orbital (HOMO), and insertion of electrons in the lowest unoccupied molecular orbital (LUMO), was studied using voltammetric data. Energy levels were calculated assuming the normal hydrogen

electrode (NHE) is $4.5\ \text{eV}$ vs. vacuum level and a potential of $0.21\ \text{V}$ for Ag/AgCl vs. NHE. Thereby, the energy of the HOMO was obtained by adding $4.71\ \text{V}$ to the measured E_{ox} (onset) and the energy of the LUMO by adding $4.71\ \text{V}$ to the measured E_{red} (onset).^{48,49} Figure S5b shows the HOMO and LUMO energies calculated from onset red/ox potentials for all investigated films. The electrochemical bandgap (E_g) of PPy-IL, PPy-DS, PPy-IL-DS, and PPy IL-DS-AuNP films was calculated to be $0.64\ \text{eV}$, $0.61\ \text{eV}$, $0.51\ \text{eV}$, and $0.46\ \text{eV}$, respectively. The higher E_g of PPy-IL indicates a lower molecular ordering and conjugation length, which may be related to steric hindrance of the IL molecule. The combination of IL and DS in PPy-IL-DS resulted in a reduction of the electrochemical band gap of PPy compared to PPy-IL and PPy-DS films, probably due to changes in the electronic band structure of PPy-IL-DS, while a larger surface facilitates charge carrier diffusion. A subtle decrease in band gap is observed for the film containing gold nanoparticles compared to PPy-IL-DS. This may be due to an effect of AuNP on the electronic structure of PPy. The presence of gold nanoparticles may avoid the charge motion limitation due to the chain length, facilitating electron transfer, improving conduction by hopping due to good conductivity, increasing the conduction path, and allowing charge accumulation on the modified electrode surface.^{4,50}

Electrochemical impedance spectroscopy (EIS) of PPy films

EIS measurements were performed in $0.1\ \text{mol L}^{-1}\ \text{LiClO}_4$ under illumination (Figure 4). The real part of impedance is highest for PPy-IL and lowest for PPy-IL-DS-Au. EIS spectra were fit to an equivalent circuit (inset of Figure 4; where R_s , R_1 , and R_2 represent uncompensated resistance, pore resistance, and charge transfer resistance, respectively.⁵¹ CPE_1 and CPE_2 represent constant phase elements attributed to the capacitance of the PPy film and the double layer, respectively. Values obtained from circuit fitting are compared in Table 2.

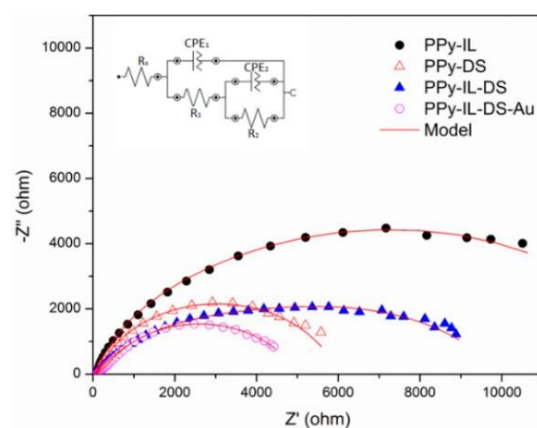


Figure 4. Nyquist plots of the PPy films acquired in $0.1\ \text{mol L}^{-1}\ \text{LiClO}_4$. The inset displays the equivalent circuit used to fit the EIS data.

Table 2. The values of the circuit elements obtained from the equivalent circuit fitting.

Sample	R_s (Ω)	CPE ₁		R_1 (Ω)	CPE ₂		R_2 (Ω)
		Q_1 (μ F)	n		Q_2 (μ F)	n	
PPy-IL	83.4	27.8	0.85	7053.1	91.8	0.68	7168.2
PPy-DS	69.3	3.66	0.84	28.8	31.6	0.78	6020.2
PPy-IL-DS	66.3	7.20	0.63	5981.1	73.9	0.57	4568.2
PPy-IL-DS-Au	86.7	13.7	0.65	442.6	7.02	0.79	4577.6

According to the literature, R_1 describes the pore resistance. PPy-IL presents the highest value of R_1 , followed by PPy-IL-DS and PPy-IL-DS-Au, and PPy-DS being the lowest (Table 2). SEM images of Figure 1a clearly demonstrate large granules separated by larger distances for the PPy-IL film. On the other hand, PPy-DS granules are closely packed and the film is smooth. R_1 is significantly decreased due to the presence of Au NPs in the PPy-IL-DS-Au film showing that the presence of Au is adventitious to decreasing pore resistance. The decrease in impedance for this film can be related to the high conductivity of the Au nanoparticles.^{52,53} Furthermore, PPy-IL films show the highest charge transfer resistance (R_2). Compared to other films the PPy-IL surface was the roughest (Figure 1a.), which may hinder charge transportation due to trap sites and ion transportation in the pores by diffusion.^{52,53} Compared to PPy-DS, R_2 is decreased when IL is used in the synthesis of PPy-IL-DS film. PPy-IL-DS-Au had similar R_2 values to PPy-IL-DS. These results suggest that interfacial charge transfer resistance is decreased when PPy films are synthesised in IL and DS mixture showing the synergistic effect of IL and DS. On the other hand, the presence of Au decreases pore resistance but does not affect charge transportation significantly.

Electrocatalytic Activity for I^-/I_3^-

The relationships between ion diffusivity, reaction kinetics, and electrochemical catalytic activity of the PPy films were tested using I^-/I_3^- , a frequently used redox couple to assemble DSSCs. In the cyclic voltammograms presented in Figure 5, the redox peaks (identified with asterisks), are attributed to the I^-/I_3^- redox reaction. Higher current densities, as well as peak areas corresponding to the coulometric charge of the I^-/I_3^- were obtained for PPy-IL-DS and PPy-IL-DS-AuNP films (Figure 5). This result is related to the larger surface area of PPy-IL-DS compared to PPy-DS and PPy-IL, and the higher roughness of PPy-IL-DS-AuNP (Figure 1), which favours ion diffusion. In addition, the presence of AuNP can improve electron transfer kinetics and/or electrocatalytic activity for the I^-/I_3^- in the polypyrrole film.⁵⁴ We suggest that the improved electrochemical activity results from the combination of a larger surface area and a high electrical conductivity, which demonstrates that PPy-IL-DS and PPy-IL-DS-AuNP are interesting counter-electrode materials for DSSC.

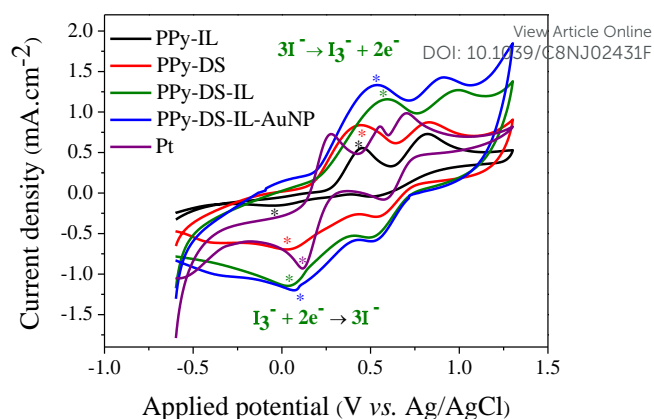


Figure 5. Voltammograms of I^-/I_3^- redox reaction at a scan rate of 20 mV s^{-1} on PPy-IL, PPy DS, PPy-IL-DS, and PPy IL DS AuNP films in acetonitrile solution containing $0.1 \text{ mol L}^{-1} \text{ LiClO}_4$, $10.0 \text{ mmol L}^{-1} \text{ NaI}$, and $1.0 \text{ mmol L}^{-1} \text{ I}_2$.

Performance of DSSCs based on Pt, PPy-IL, PPy-DS, PPy-IL-DS, and PPy-IL-DS-AuNP CEs

Figure 6 displays the J-V curves of DSSCs based on PPy counter electrodes (CEs). For comparison DSSC assembled with Pt as a CE is also presented. The highest fill factor (FF), open circuit potential (V_{oc}) value, and efficiency (η %) were obtained for Pt (Table 3). In terms of FF, the PPy films follow the order: PPy-IL-DS-AuNP > PPy-IL-DS > PPy-DS > PPy-IL. These results show that PPy-IL offers the highest resistance, in agreement with the EIS data (Table 2), whereas R_2 was highest for PPy-IL and lowest for PPy-IL-DS and PPy-IL-DS-Au. However, the photocurrent for PPy-IL-DS was slightly higher than that obtained from PPy-IL-DS-AuNP, which might be due to the slightly higher thickness of PPy-IL-DS-AuNP. In addition, there was a slight change in the V_{oc} values of PPy based CE as compared to Pt CE. The literature reports CE based V_{oc} difference for the same electrolyte.⁵⁵

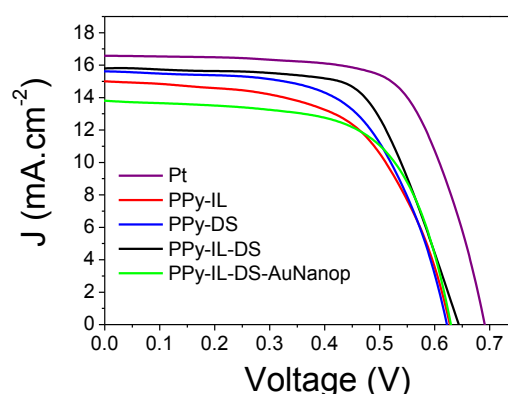


Figure 6. Current versus potential for the DSSCs using the Pt, PPy IL, PPy DS, PPy-IL-DS, and PPy-IL-DS-AuNP films as counter electrodes.

Hence, doping PPy in the presence of IL or in combination with other surfactant salts is a potential method to obtain PPy based CEs. Based on properties such as high electrochemical and chemical stability, wide electrochemical potential window, hydrophobicity, and low cost, doped-PPy-based CEs are a very promising alternative for DSSC. These results show that PPy-IL-DS and PPy-IL-DS-AuNP films are promising DSSC CE materials, with responses comparable to Pt and other PPy CEs.⁵⁴⁻⁵⁸ However; further efforts are required to optimise the composition of nanocomposites and film thicknesses.

Table 3. Photovoltaic parameters of the DSSCs with Pt, PPy-IL, PPy-DS, PPy-IL-DS, and PPy IL-DS-AuNP films as counter-electrodes.

Counter Electrodes	J _{sc} (mAcm ⁻²)	V _{oc} (mV)	FF (%)	η (%)
Pt	16.6	0.69	67	8.2
PPy-IL	15.0	0.63	58	5.4
PPy-DS	15.7	0.63	60	6.1
PPy-IL-DS	15.9	0.65	62	7.1
PPy-IL-DS-AuNP	13.8	0.63	62	4.6

Conclusion

In summary, we have synthesized PPy films, with interesting electrochemical behaviour, in the mixture of IL and DS. The ionic liquid BMI.CH₃SO₃ can drive the oxidation state of the polypyrrole chains, resulting in a film presenting a high concentration reduced pyrrole rings; on the other hand, the presence of DS results in a PPy film with high concentration of bipolaron states. By mixing the IL and DS a PPy film presenting mainly polaronic states was obtained. The morphology, conductivity, and electrocatalytic properties of the PPy films, were ultimately controlled by the presence of the IL that behaves as an entropic driver. The electrocatalytic activity of the counter electrodes is mainly determined by the oxidation state of the polypyrrole. The study of PPy-IL-DS and PPy-IL-DS-AuNP based counter electrodes for DSSC is proposed for the first time and the results show great potential application in flexible dye sensitised solar cells.

There are no conflicts to declare.

Acknowledgements

The authors gratefully acknowledge funding support, scholarships, and fellowships from Conselho Nacional de Desenvolvimento Científico e Tecnológico (CNPq), Brazil, and Coordenação de Aperfeiçoamento de Pessoal de Nível Superior (CAPES). They are thankful to the Center of Microscopy and Microanalysis (CMM-UFRGS) for the SEM images. etc.

- Liu R.; Wang J. W.; Sun T.; Wang M.; Wu C.; Zou H.; Song T.; Zhang X.; Lee S. T.; Wang Z. L.; Sun B. *Nano Lett.* 2017, **17**, 4240-4247.
- Sun J.; Shu X.; Tian Y.; Tong Z.; Bai S.; Luo R.; Li D.; Chen A. *Sens. Actuators B-Chem.* 2017, **238**, 510-517.
- Jeon S. S.; Kim C.; Ko J.; Im S. S. *J. Phys. Chem. C* 2011, **115**, 22035-22039.
- Mianqi X.; L. Fengwang; Chen D.; Yang Z.; Wang X., Ji J. *Adv. Mater.* 2016, **28**, 8265-8270.
- Ferreira J.; Giroto E. M. 2009, **137**, 426-431.
- Ferreira J.; Giroto E. M. *J. Braz. Chem. Soc.*, 2010, **21**, 312-318.
- Pattananuwat P.; Aht-ong D. *Electrochim. Acta*, 2017, **224**, 149-160.
- Loguercio L. F.; Alves C. C.; Thesing A.; Ferreira J. *Phys. Chem. Chem. Phys.* 2015, **17**, 1234-1240.
- Qiu L.; Liu B.; Peng Y.; Yan F. *Chem. Commun.* 2011, **47**, 2934-2936.
- Ferreira J.; Santos M. J. L.; Matos R.; Ferreira O. P.; Rubira A. F.; Giroto E. M.; J. *Electroanal. Chem.* 2006, **591**, 27-32.
- Liu J.; Gu M.; Ouyang L.; Wang H.; Yang L.; Zhu M.; *ACS Appl. Mater. Interfaces*, 2016, **13**, 8502-8510.
- Liu J.; Wen Y.; van Aken P. A.; Maier J.; Y Yan.; *J. Mater. Chem. A* 2015, **3**, 5259.
- Wu M.; Lin X.; Wang Y.; Wang L.; Guo W.; Qi D.; Peng X.; Hagfeldt A.; Grätzel M.; Ma T. *J. Am. Chem. Soc.* 2012, **134**, 3419-3428.
- Heintges G. H. L.; Leenaers P. J.; Janssen J. A. R. *J. Mater. Chem. A* 2017, **5**, 13748-13756.
- Hwang D. K.; Song D.; Jeon S. S.; Han T. H.; Kang Y. S.; Im S. S. *J. Mater. Chem. A* 2014, **2**, 859-865.
- Brédas J.; Silbey R.; Boudreaux D.; Chance R. *J. Am. Chem. Soc.* 1983, **105**, 6555-6559.
- Santos M. J. L.; Brolo A.; Giroto E. *Electrochim. Acta*. 2007, **52**, 6141-6145.
- Otero T.F.; Grande H.; Rodríguez J. J. *J. Electroanal. Chem.* 1995, **394**, 211-216.
- Kaufman J. H.; Colaneri N.; Scott J. C.; Street G. B. *Phys. Rev. Lett.* 1984, **53**, 1005-1008.
- Lin X.; Li J.; Smela E.; Yip S. *Int. J. Quantum Chem.* 2005, **102**, 980-985.
- Brédas J. L.; Scott J. C.; Yakushi K.; Street G. B. *Phys. Rev. B* 1984, **30**, 1023-1025.
- Brédas J. L.; Chance R. R.; Silbey R. *Phys. Rev. B*, 1982, **26**, 5843-5854.
- Håkansson E.; Lin T.; Wang H.; Kaynak A. *Synth. Met.* 2006, **156**, 1194-1202.
- Yamaura M.; Hagiwara T.; Iwata K. *Synth. Met.* 1988, **26**, 209-224.
- Patil A. O.; Heeger A. J.; Wudl F. *Chem. Rev.*, 1988, **88**, 183-200.
- Banerjee C.; Mandal S.; Ghosh S.; Kuchlyan J.; Kundu N.; Sarkar N. *J. Phys. Chem. B* 2013, **117**, 3927-3934.
- Anderson J. L.; Pino V.; Hagberg E. C.; Sheares V. V.; Armstrong D. W. *Chem. Comm.* 2003, **19**, 2444 2445.
- Miskolczy Z.; Sebok-Nagy K.; Biczók L.; Göktürk S. *Chem. Phys. Lett.* 2004, **400**, 296-300.
- Deepa M.; Ahmad S.; *Eur Polym J.* 2008, **44**, 3288-3299.
- Kong S.; Fontaine O.; Roche J.; Bouffier L.; Kuhn A.; Zigah D.; *Langmuir*, 2014, **30**, 2973-2976.
- Porcher M.; Esnault C.; Tran-Van F.; Ghamous F.; *J. Appl. Electrochem.* 2016, **46**, 1133-1145.
- Gao W.; Sel Ozlem.; Perrot, H.; *Electrochim. Acta*. 2017, **10**, 262-273.
- Peres R. C.; Pernaut J. M.; De-Paoli, M-A.; *J. Polym. Sci., Part A: Polym. Chem.* 1991, **29**, 225-231.
- Funkhouser G. P.; Arevalo, M. P.; Glatzhofer D. T.; O'Rear E. A.; *Langmuir*, 1995, **11**, 1443-1447.

ARTICLE

Journal Name

- 35 Chen L. G.; Strassburg S. H.; Bermudez H. J. *Colloid Interface Sci*, 2016, **477**, 40-45.
- 36 Omastová M.; Trchová M.; Kovářová J.; Stejskal J. *Synth. Met.* 2003, **138**, 447-455.
- 37 Antonietti M.; Kuang D.; Smarsly B.; Yong Z. *Angew. Chem. Int. Ed.* 2004, **43**, 4988-4992.
- 38 Chang M.; Kim T.; Park H.-W.; Kang M.; Reichmanis E.; Yoon H. *ACS Appl. Mater.* 2012, **4**, 4357-4365.
- 39 Zhang X.; Yan X.; Guo J.; Liu Z.; Jiang D.; He Q.; Wei H.; Gu H.; Colorado H. A.; Zhang X.; Wei S.; Guo Z. *J. Mater. Chem. C* 2015, **3**, 162-176.
- 40 Dupont J., Scholten D. *J. Chem. Soc. Rev.* 2010, **39**, 1780-1804.
- 41 Tabačiarová J.; Mičušík M.; Fedorko P.; Omastová M. *Polym. Degrad. Stab.* 2015, **120**, 392-401.
- 42 Gong F.; Xu X.; Zhou G.; Wang Z. S. *Phys. Chem. Chem. Phys.* 2013, **15**, 546-552.
- 43 Ma X.; Zhao S.; Zhang S. *New Mat. Electrochem. Systems.* 2017, **20**, 13-20.
- 44 Rodríguez I.; Scharifker B. R.; Mostany J. *J. Electroanal. Chem.* 2000, **491**, 117-125.
- 45 Wang J.; Neoh K.; Kang E. *Thin Solid Films.* 2004, **446**, 205-217.
- 46 Park J.; Lee S.; Kim B.; Park Y. W. *Appl. Phys. Lett.* 2002, **81**, 4625-4627.
- 47 Yuan L.; Yao B.; Hu B.; Huo K.; Chen W.; Zhou J. *Energ. Environ. Sci.* 2013, **6**, 470-476.
- 48 Johansson T., Mammo W., Svensson M., Andersson M. R., Inganäs O. *J. Mater. Chem.* 2003, **13**, 1316-1323.
- 49 Hou J.; Tan J.; Yong Y.; He Y.; C Yang.; Li Y. *J. Am. Chem. Soc.* 2006, **128**, 4911-4916.
- 50 Singh S.; Jain D. V. S.; Singla M. L. *Anal. Methods.* 2013, **5**, 1024-1032.
- 51 El Jaouhari A.; Laabd M.; Bazzaoui E. A.; Albourine A.; Martins J. I.; Wang R.; Nagy G.; Bazzaoui M. *Synth. Metals.* 2015, **209**, 11-18.
- 52 Bisquert J.; Belmonte G. G.; Santiago F. F.; Compte A. *Electrochem. Commun.* 1999, **1**, 429-435.
- 53 Chen W.; Li C. M.; Chen P.; Sun Q. C. *Electrochim. Acta*, 2007, **52**, 2845-2849.
- 54 Marchesi L. F. Q. P.; Simões F. R.; Pocrifka L. A.; Pereira E. C. *J. Phys. Chem. B*, 2011, **115**, 9570-9575.
- 55 Wu j.; Lan Z.; Lin J.; Huang M.; Huang Y.; Fan L.; Luo G.; Lin Y.; Xie Y.; Wei Y.; *Chem. Soc. Rev.*, 2017, **46**, 5975-6023.
- 56 Lim S. P.; Pandikuma A.; Lim S. Y.; Huang N. M.; Lim H. N. *Sci. Rep.* 2014, **4**, 5305 (1 7).
- 57 Hou W.; Xiao Y.; Han G.; Zhou H. *Electrochim. Acta.* 2016, **190**, 720-728.
- 58 Peng T.; Sun W.; Huang C.; Yu W.; Sebo B. B.; Dai Z.; Guo S.; Zhao Z. *Appl. Mater. Interfaces.* 2014, **6**, 14-17.

View Article Online
DOI: 10.1039/C8NJ02431F

